MICROSCOPIC STUDIES OF FIELD EMISSION FROM RF CAVITY SURFACES

R. J. NOER

Physics & Astronomy Dept., Carleton College, Northfield, MN 55057

Abstract: During the last two or three years, new kinds of experiments have been carried out that allow for the first time the direct microscopic observation, before and after electron field emission takes place, of RF cavity surfaces and emission sites. This review paper describes the apparatus and techniques that have been used, and summarizes the results obtained for naturally occurring emission sites as well as for sites intentionally introduced in the form of irregular Fe particles.

1 INTRODUCTION

For many years, enhanced field emission (FE) has constituted a major barrier to the attainment of the high accelerating fields that should be possible with superconducting radio-frequency particle accelerator cavities[1]. However, the very nature of these high-Q resonant cavities has made real-time direct and local observation of individual emission sites difficult. Most of the considerable body of evidence and experience related to such sites has been obtained either indirectly (e.g., via the externally sensed heating of the cavity walls from the emitted electrons as they are accelerated by the cavity fields and strike the walls) or integrally (e.g., by the drop in cavity Q as the electrons emitted simultaneously from an unknown number of sites load its performance). Recently, however, new kinds of cavities designed specially for field emission research, and new kinds of observations on traditional accelerating cavities, have made possible new kinds of microscopic observations of emission sites—in one case in real time, and in the others after-the-fact but locally. These observations, coupled with ongoing studies of DC field emission[2-4], allow one for the first time to begin constructing a realistic model of how such emission sites behave in RF cavities, and at the same time suggest some important directions to pursue in seeking to prepare reduced-emission cavities.

In this paper our current knowledge of the structure and operation of RF field emission sites will be reviewed, with particular emphasis on the work of the last two or three years. Section 2 begins by examining the apparatus and kinds of measurements that have been particularly fruitful in providing new insights. In sections 3 and 4 the results of those measurements are reviewed, and in section 5 we draw some conclusions from these results.

2 APPARATUS AND METHODS

Recent advances in the microscopic understanding of RF field emission have come from three kinds of apparatus in two laboratories. We begin by examining each in turn.

2.1 The mushroom cavity

Cornell's "mushroom" cavity[5] (so called from its characteristic shape) is shown in Fig. 1(a). Constructed entirely of niobium, it features a removable end plate with a bump or inverted "dimple" at its center. The geometry of the cavity is such that the electric field at the center of the dimple is very much greater than that anywhere else (see Fig. 1(b)); thus if field emission occurs in the cavity, the site or sites responsible for it are very much more likely to be on the dimple than anywhere else. One can characterize the relevant area of the dimple as that where the field is >80% of the maximum value, namely 40 mm^2. The maximum fields attainable surpass 100 MV/m.

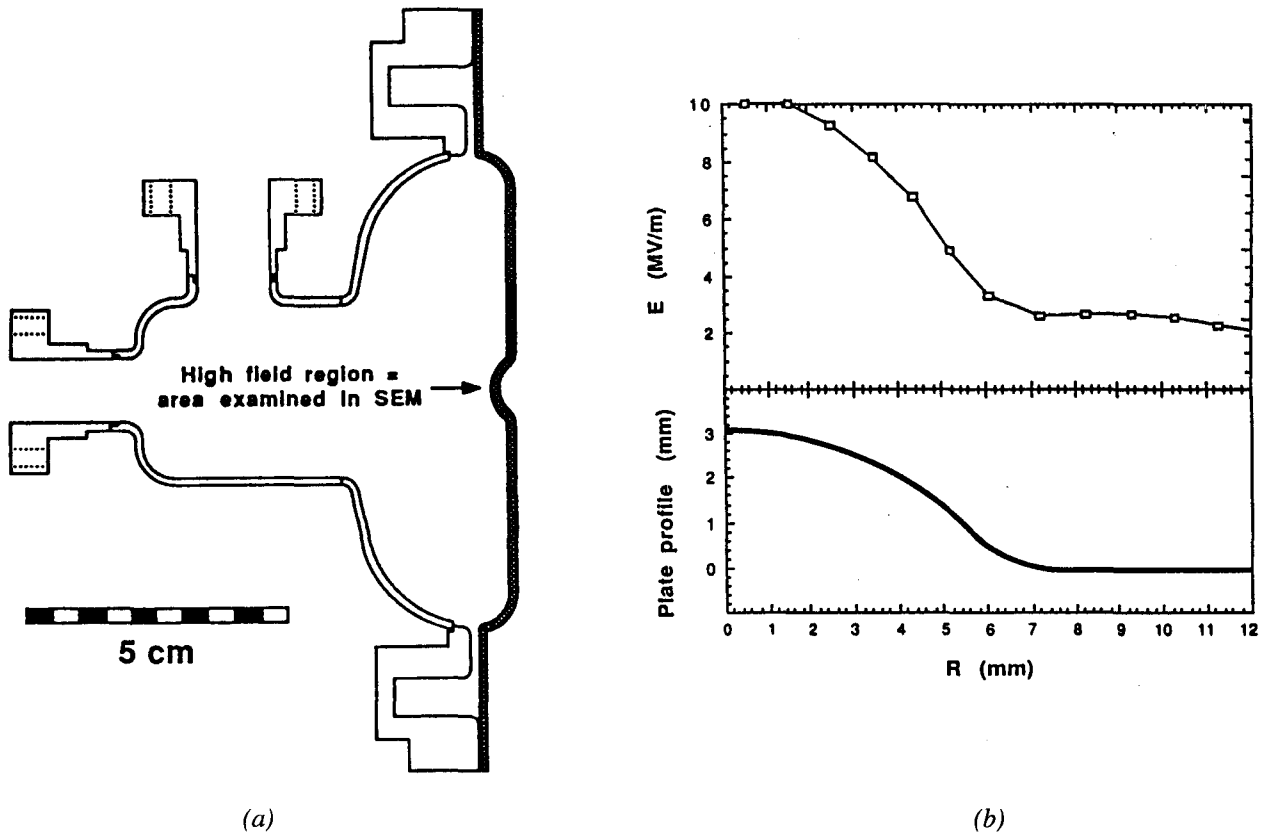

(a) *(b)*

Figure 1: Cornell mushroom cavity. (a) Cavity geometry, (b) surface electric field on cavity endplate.

A typical experimental run with this cavity might be as follows: A freshly cleaned end plate is clean-room mounted on the cavity, which is then cooled in superfluid helium. RF power (6 GHz) is coupled to the cavity, and the input level slowly raised while the cavity Q and internal field are monitored along with any x-ray emission and antenna current that signal the onset of FE. At some opportune point the run is terminated and the cavity warmed. The end plate is then removed in a clean room and transferred directly to a SEM located in the same clean room. It is then scanned for unusual morphological features and their elemental composition (with the SEM's EDX facility). When results warrant, an end plate can be transported to off-site Auger analysis or atomic force microscope facilities, though physical limitations of these facilities requires cutting the dimple from the rest of the end plate, preventing further RF testing.

As will be discussed in more detail below, the mushroom cavity was the first to provide high-resolution microscopic views of an interior RF cavity region where FE was known to have taken place[6].

2.2 The Thomson cavity

Saclay's "Thomson" cavity[7] (so called after the manufacturer supporting the work) was inspired by the mushroom cavity, but is different in several significant ways. Figure 2(a) shows its geometry; the cavity is constructed of Cu-plated stainless steel with a Nb "finger". Like the dimple of the mushroom end plate, the Thomson finger provides a local region where the cavity field is considerably enhanced (see Fig. 2(b)) and where FE is thus most likely to occur. The area where the field is >80% of the maximum value is approximately 12 mm^2. The finger can be easily unscrewed for microscopic observation.

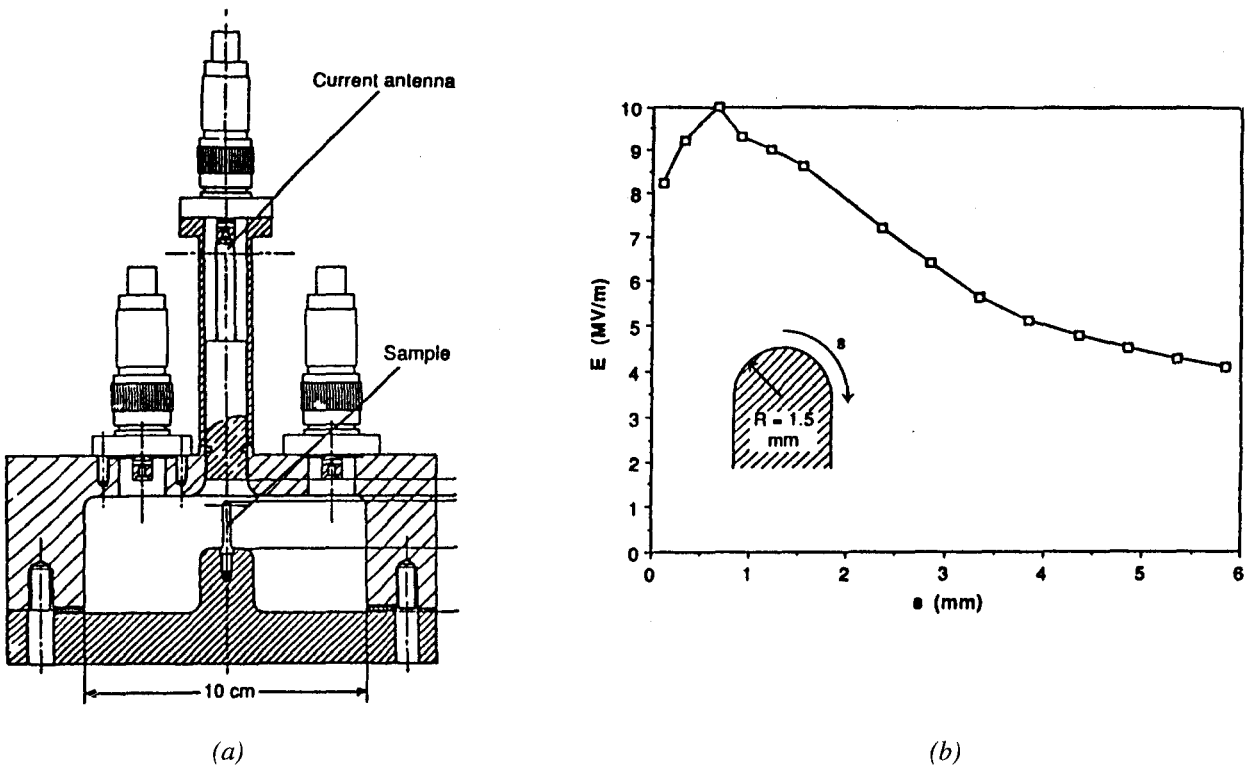

Figure 2: Saclay Thomson cavity. (a) Cavity geometry, (b) surface electric field on cavity finger.

Typically, an experiment begins with examination of a freshly prepared Nb finger in a SEM equipped as a DC field emission scanning microscope (FESM)[3]. With the latter, the finger's surface is scanned for emission sites, and any sites thus found can be measured for their characteristics (emission threshold, Fowler-Nordheim enhancement factor and area[1]) and photographed with high SEM resolution. In some cases, lower resolution SEM photos are also made of the entire high-field surface. Under dust-free conditions, the finger is then screwed into place in the cavity, and the cavity sealed with an In O-ring. The assembly is RF-tested (1.5 GHz) at room temperature, with Q and internal E monitored as the input power is slowly increased; at the same time emission current (known from electron trajectory calculations to originate from the central

7 mm^2) is collected on a probe and monitored. At some chosen point, the run is terminated, and the finger is removed and returned to the SEM for morphological and elemental (EDX) examination and DC emission measurement. The technique has made it possible for the first time to make comparisons of RF and DC field emission characteristics of individual emission sites.

As the Thomson cavity is normally operated at room temperature, the turn-around time of an experiment is much shorter than with the mushroom cavity. A price paid, however, is that dissipation in the Cu walls limits the maximum field achievable to about 50 MV/m.

A Thomson cavity has recently been modified for optical measurements by the addition of a window opposite the Nb finger[8] (Fig. 3). One pixel on the CCD camera corresponds to 3.6 μm on the finger surface; the window allows quantitative measurements of light intensity by the photomultiplier of a region as small as 0.25 mm in diameter. The arrangement has allowed the first real-time observations of the intensity and spectrum of optical radiation from RF electron emission sites.

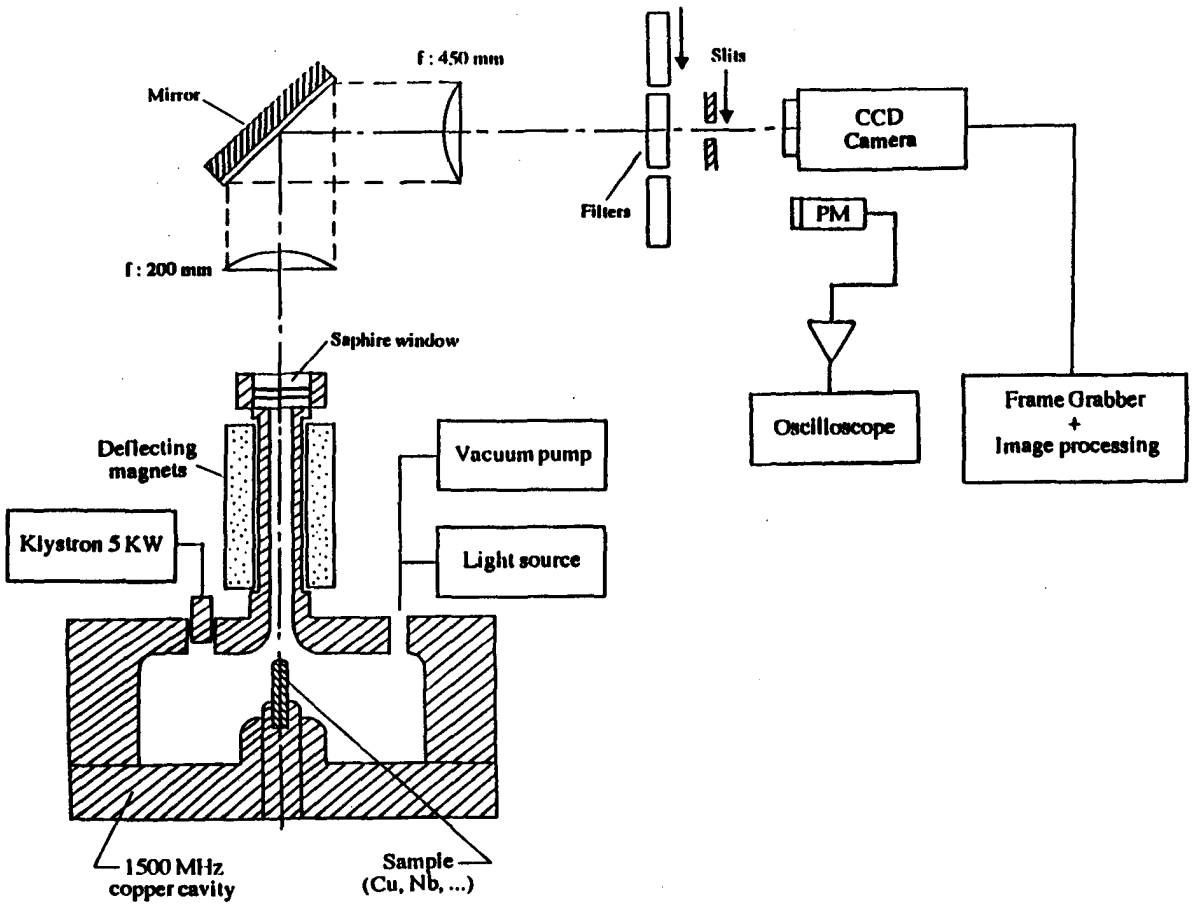

Figure 3: Thomson cavity modified for optical measurements.

2.3 Dissection of S-band cavities

A program at Cornell where conventional single-cell S-band (3-GHz) cavities are cut apart for high-resolution microscopic examination has provided new information[9] about the processing of RF field emission sites. A cavity, fitted with a temperature diagnostic system[10] (Fig. 4), is conventionally tested at RF in both the normal CW regime and using high peak power processing. At some point in the test, when a particular field level has been reached, or when Q or T measurements suggest that a significant event (e.g., a processing event) has occurred, the test is ended and the cavity is carefully cut apart so as to allow direct SEM observation of its interior high-field walls. The sacrifice of these cavities has provided the first instances where high-resolution microscopic examination has been made of individual sites specifically associated with RF field emission in an accelerating cavity.

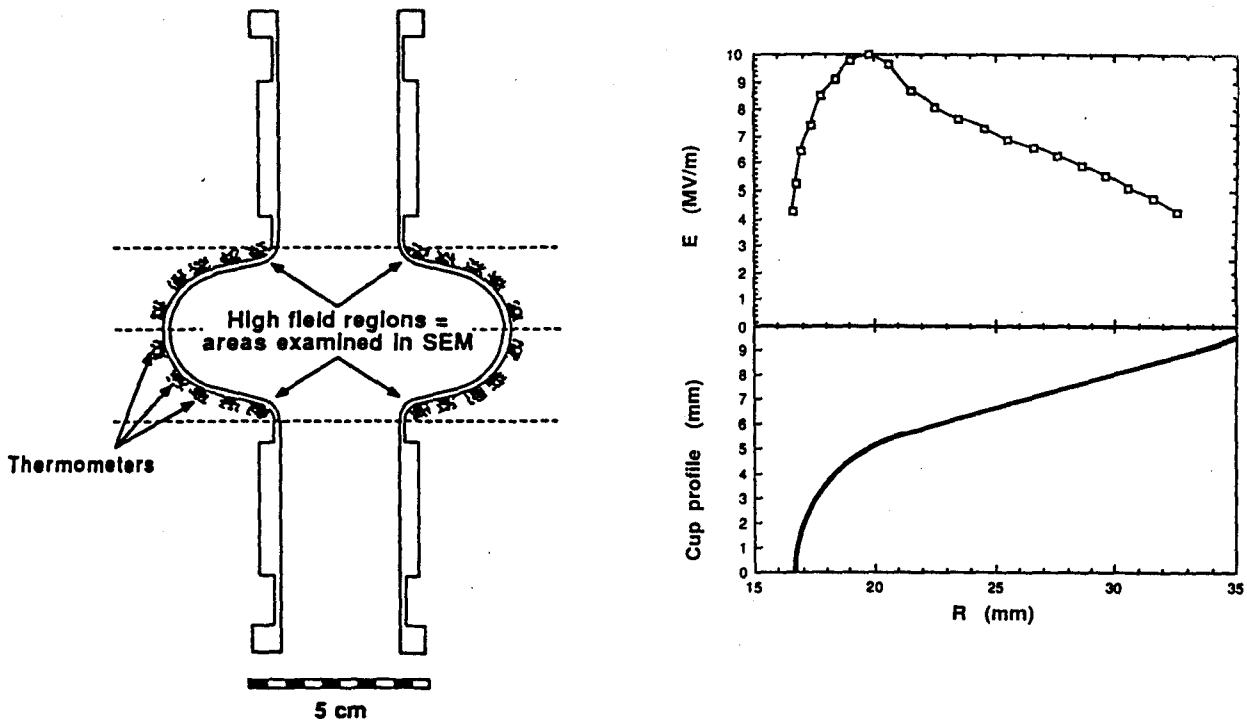

Figure 4: Cornell S-band cavity. (a) Cavity geometry, (b) surface electric field near iris.

3 SITES ON CLEAN SURFACES

In RF as well as in often in DC, the ultimate fate of a field emission site driven hard enough appears to be the appearance of one or more of several characteristic features: craters, starbursts, and ripples. In this section we discuss each in turn, focusing on the new information provided by the above-described experimental facilities and techniques.

3.1 Starbursts

While probably not the most fundamental of these features, the starburst has often proved the most convenient means of locating the site of a violent event on a surface previously exposed to RF. Figure 5 shows a typical example, from a mushroom cavity endplate[6]. The starburst's dark appearance in an SEM, its characteristic pointed shape, and its considerable size (typically 100 μm in the mushroom cavity) make it easy to spot on a large surface where the discovery of other emission-related features would be considerably more difficult and tedious.

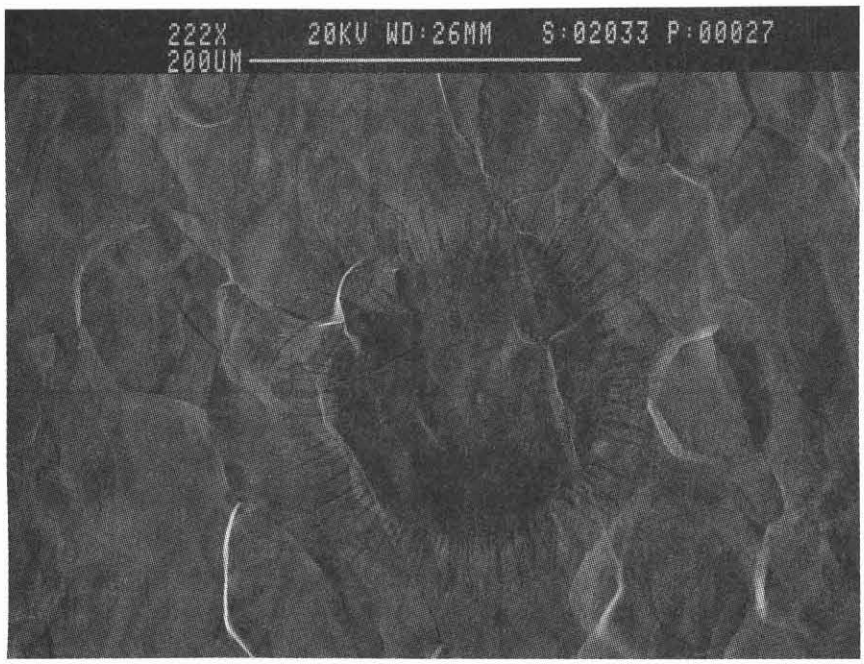

Figure 5: Typical starburst, found on mushroom cavity endplate.

Starbursts were first seen on mushroom cavity endplates; typically anywhere from one to several tens are found, depending on the conditions of the preceding RF test; in general, the higher the RF field, the larger the number of starbursts. They are also found on dissected S-band cavities[9] and, on certain samples, in DC FE measurements at the location of a spark (set off either by a field emitting particle or simply by the close approach of a pointed high-voltage anode to a clean cathode surface)[11]. They have not been seen on Thomson cavity fingers; however, this may simply reflect the lower maximum field achievable in that cavity.

A starburst is always associated with some kind of much smaller central feature, usually a crater (see below), and one assumes that it is a side-effect of that feature (e.g., a trace left by a plasma cloud resulting from the explosive destruction of a former emission site). Its particular appearance can vary considerably, from a compact dark sphere with a dense fringe of short rays at its surface, to a feature composed almost entirely of longer discrete rays and very little central core. Two or more starbursts are commonly seen superposed, suggesting sequential formation. For a particular type of cavity, one finds a certain range of starburst diameters, but in general those on mushroom endplates (6 GHz) are smaller (~100 μm) than those on S-band cavities (~200 μm). (DC starbursts tend to be smaller—10-40 μm—though this may be related to the small anode-cathode gaps used in creating them[11].)

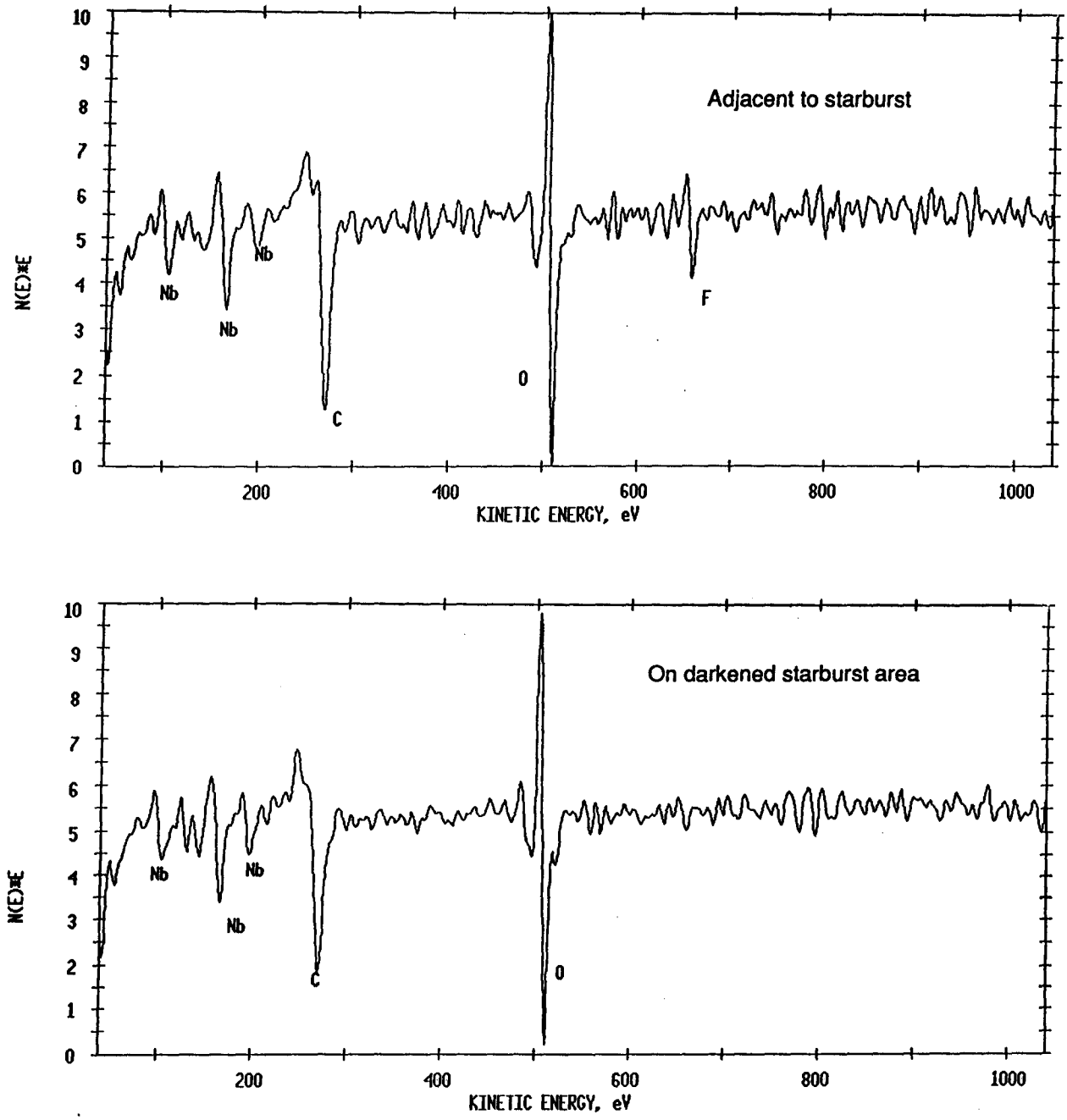

Figure 6: Auger scans of mushroom cavity endplate, (top) outside and (bottom) within starburst.

While examination of starbursts with EDX failed to reveal any associated variation in surface composition, Auger measurements on mushroom endplates have proved more revealing[12]: As can be seen in Figures 6 and 7, a fluorine signal that is clearly present across the background Nb endplate surface is systematically missing within the dark part of the starburst. Apparently a superficial residue of F (too thin for EDX detection) is left on a Nb surface by the HF used in the standard chemical etch treatment, and is preferentially removed in a characteristic pattern by the explosion of the central site. This interpretation is supported by the Saclay experience with sparking in a FESM[11]: starbursts are easily produced on a freshly-etched Nb surface, but never

on Nb that has been exposed to air for some time (days or weeks), or on other materials that are cleaned mechanically. (Mushroom endplates are almost always etched shortly before mounting on a cavity which is then immediately evacuated.) SEM detection of starbursts using backscattered electrons (which, like Auger electrons, arise from a thinner surface layer than EDX photons and which, unlike secondary electrons, produce a contrast that is largely determined by the atomic number of that layer) also corroborates the Cornell result: the starburst image is brighter than the surrounding background, consistent with the absence of the light element F.

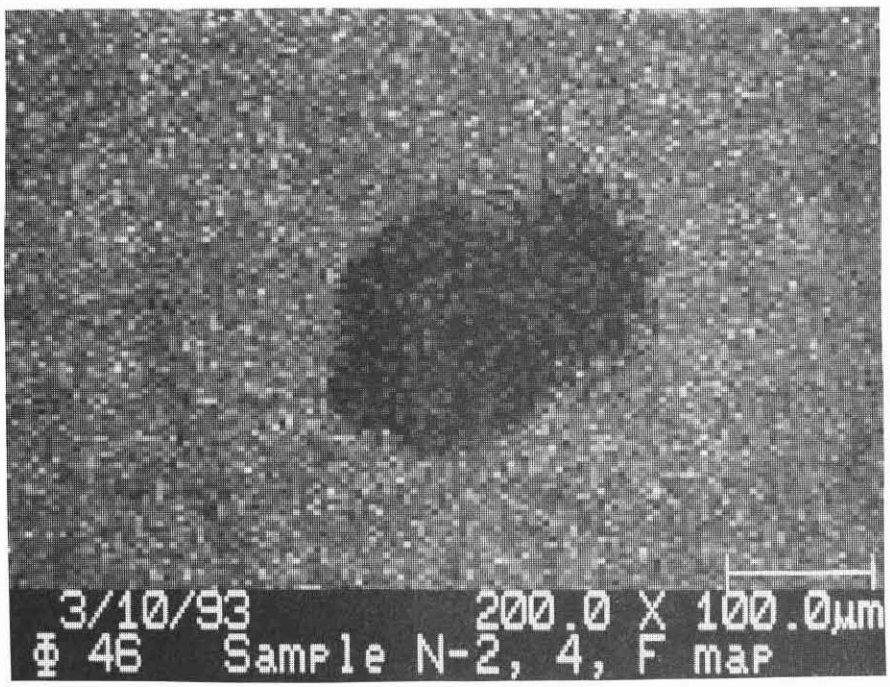

Figure 7(a) Auger fluorine map of starburst region.

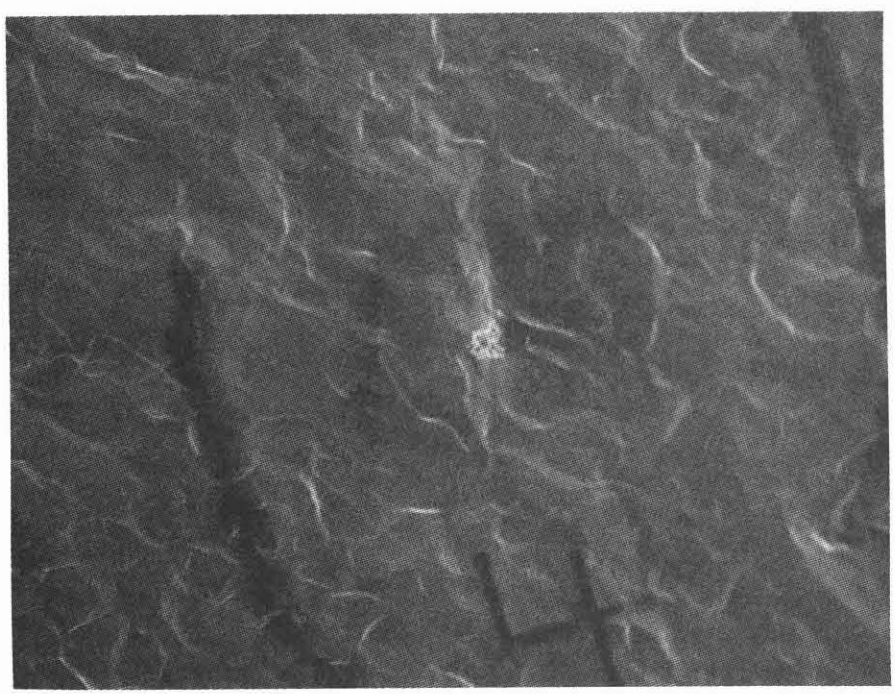

Figure 7(b): Secondary electron image of same region. (Artificial markings were added to facilitate relocation of site.)

3.2 Ripples

Wave-like ripples are frequently seen spreading out from an apparent source in or associated with a central crater (Fig. 8). Their wavelength varies by a factor of 2 or 3 over a given pattern, but their mean spacing appears to depend on RF frequency (~400 nm at 3 GHz but only ~200 nm at 6 GHz). They have been seen in mushroom and S-band cavities[6], but have not been found on Thomson fingers or in any DC work. While they produce no contrast in high-resolution Auger (and thus appear not to be produced by compositional variations), clear imaging of a mushroom endplate has been produced at Carleton using an atomic force microscope (AFM)[12]. Figure 9(a) shows an example. As the AFM's contrast results almost exclusively from geometric variations, its ability to image these ripples is strong evidence that they are physical waves in the Nb surface. Figure 9(b) shows a height profile of a slice through the region of Fig. 9(a); the peak-to-peak amplitude evident there, about 40 nm, is typical of amplitudes measured for ripple patterns.

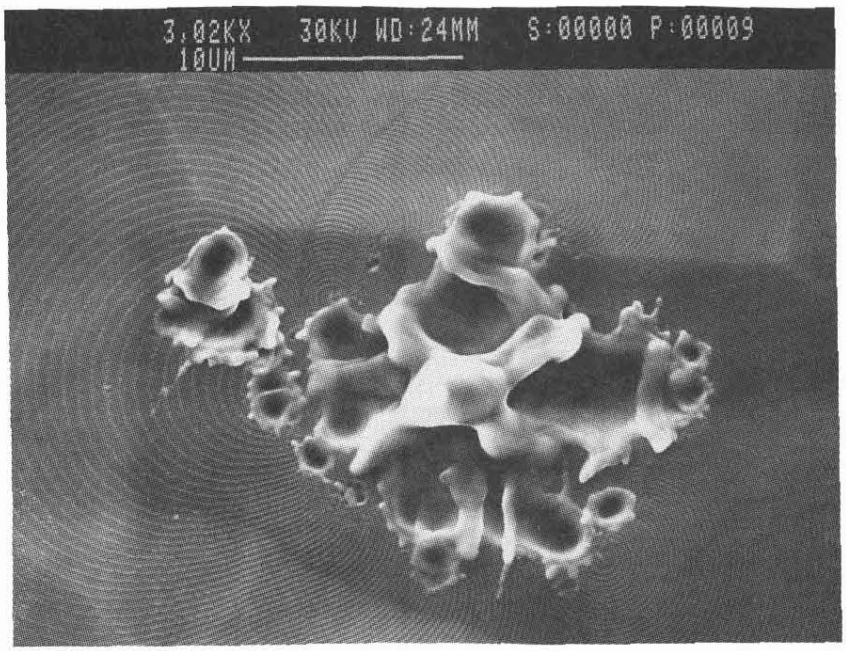

Figure 8: Ripples spreading out from central crater formation (SEM image).

Often a complex of ripples and craters suggests a sequential process: the superposition of craters over a previously created pattern of ripples. Occasionally, as in the lower right part of Fig. 8, the ripples give the clear appearance of spreading from a point source. In addition, they frequently appear to "diffract" around obstacles, and divide into separate "beams" that sometimes recombine with coherent phase. It is easy to imagine a point source oscillating in a molten surface under the influence of RF forces, generating surface tension waves that are subsequently frozen in as the surface cools through the melting point.

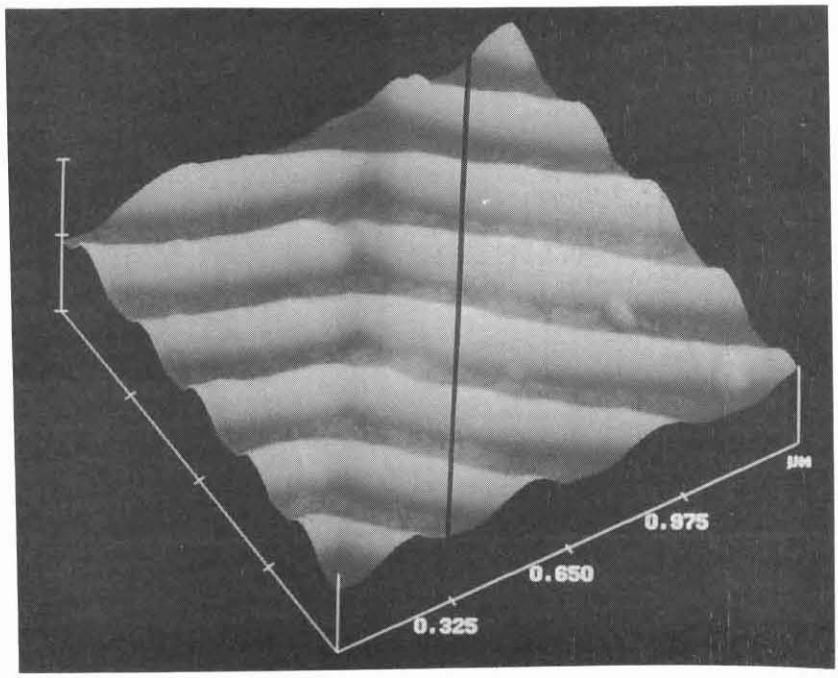

Figure 9(a): Atomic force microscope image of ripples.

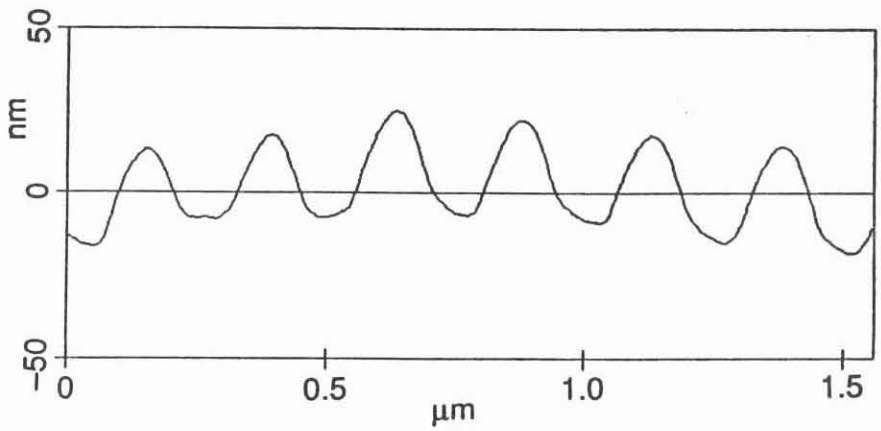

Figure 9(b): AFM height profile along line in preceding figure.

3.3 Craters

A crater, or perhaps several grouped craters, appears to be the common signal of a former (and sometimes continuing) field emission site. Well known to result from arc and spark processes in high-voltage DC vacuum discharges, these have been seen with each of the RF facilities described above. Figure 10 shows a typical crater (a more violent grouping of craters is evident in Fig. 8). Crater diameters tend to fall in a range between about 1 and 5 µm. As mentioned above, they are often located near the center of a starburst, which then serves as a convenient pointer to the crater's presence (see Figures 5 and 7(b)). When produced by a DC spark and then observed at DC in the Saclay FESM[11], craters often show FE for fields in the range of tens of MV/m.

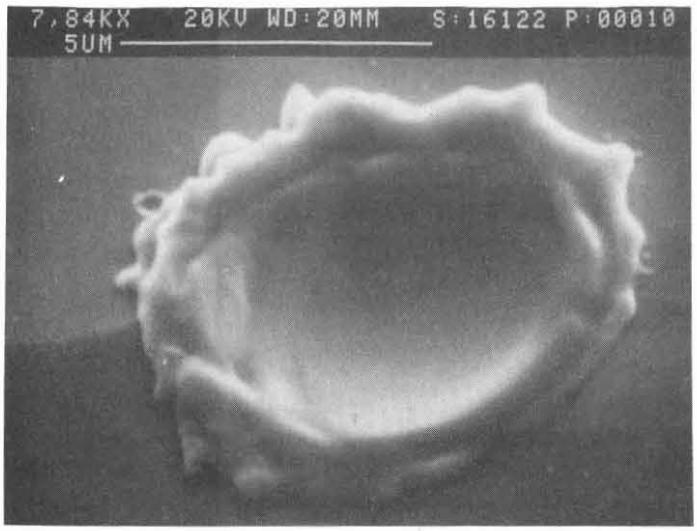

Figure 10: Typical crater, found on Thomson cavity finger.

While foreign elements were only occasionally found by EDX in craters produced during RF cavity tests, recent Auger measurements have found evidence for foreign impurities in each of 29 craters examined[12]. This finding supports the view that such craters are produced by a violent event associated with an impurity particle or inclusion on or in the cavity surface. Figure 11(a) is an Fe Auger map for a particular crater showing the concentration of the major foreign element associated with that crater; Fig. 11(b) is the corresponding SEM image. Here, as with most other craters examined, the main part of the impurity distribution is within 2 or 3 crater radii of its center. Figure 12 shows the relative frequency with which various foreign elements have been found at crater centers in mushroom endplates; most can plausibly be related to materials found in the cavity environment during assembly or operation.

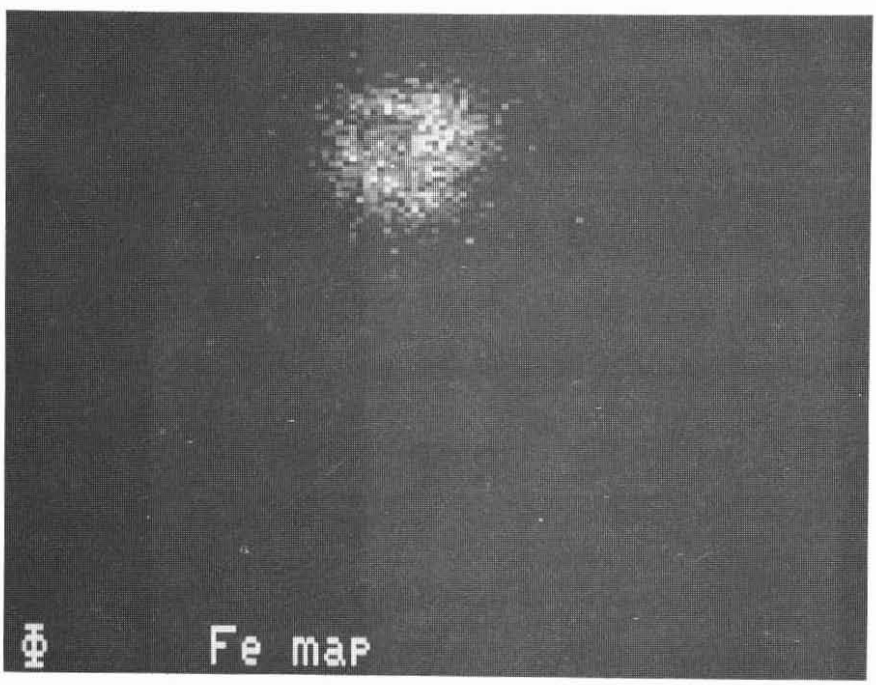

Figure 11(a): Auger Fe map of crater region

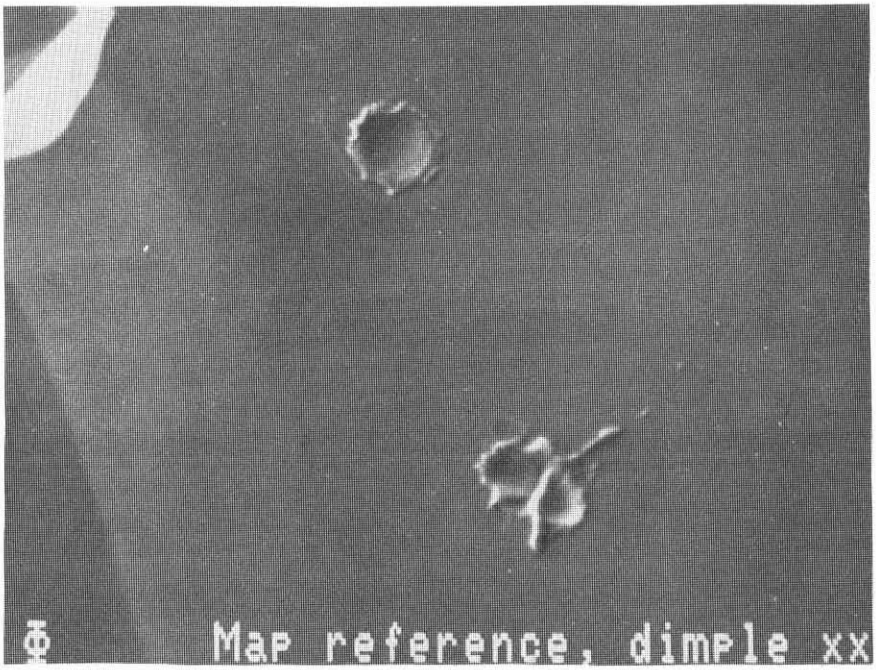

Figure 11(b) Secondary electron image of same region.

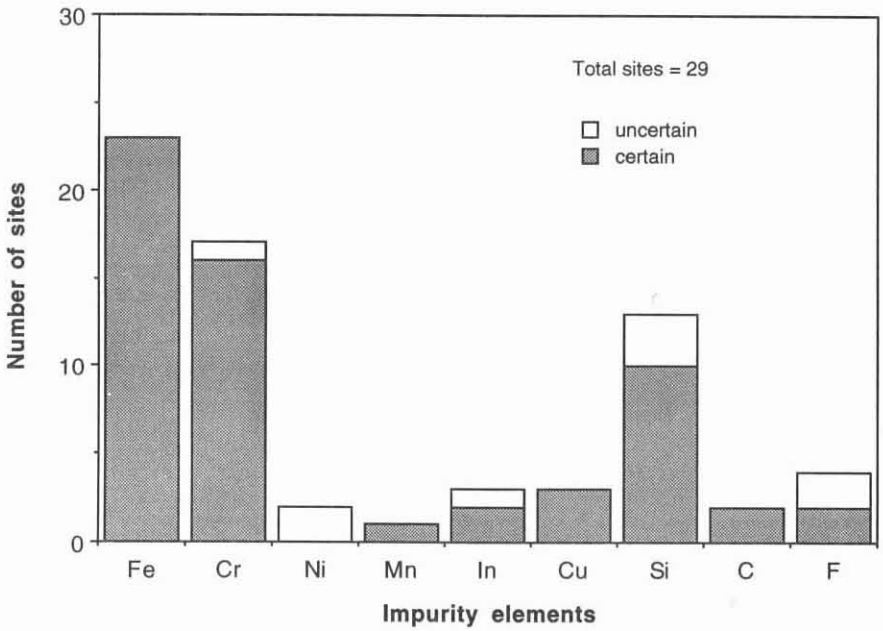

Figure 12: Relative frequency of foreign elements found in mushroom cavity craters.

One S-band test has provided a particularly clear association of a crater/starburst feature with RF FE[9]. Here a test was stopped after temperature maps had been obtained showing a single "hot" spot on the cavity wall. Electron trajectory calculations successfully modelled the temperature distribution by assuming a single emitter located at a particular position; when the cavity was cut up and that location examined in the SEM, a starburst/crater feature was found, with no other unusual features apparent in the vicinity.

4 INTENTIONALLY PRODUCED SITES

A problem with the work discussed above is that it has been difficult to examine potential emission sites in the stages before they reveal themselves by the catastrophic generation of craters and other features just discussed. Recent work with the Thomson cavity at Saclay has tried to get around this problem by intentionally introducing emission sites, hoping to learn from their behavior more about how "natural" emission sites operate and evolve.

DC measurements[3] have shown that irregularly shaped metal particles of certain elements are particularly strong emitters. A prime instance is Fe, which is also abundant in the cavity test environment and is implicated in the RF emission process by the Auger studies of craters mentioned above. To study the behavior of such particles in an RF environment, tests were carried out where irregular Fe particles were sprinkled on an otherwise emission-free Thomson cavity finger[13,14]. Photographs of the finger tip were made in the SEM to document the distribution of particles. The finger was then RF tested and found to emit at low fields. SEM examination after such a test reveals three unexpected phenomena:

1. Many of the particles have disappeared, often leaving behind a small crater. (The crater shown in Fig. 10 was produced in this manner.) The fraction of particles remaining appears to be a function of the RF pulse length; in one comparison[7], 85% were left after 10-ms pulses, but only 32% after 200-μs pulses at the same field level.

2. The remaining particles have assumed an upright position on the surface. Figure 13 shows an example; one can see there some extreme instances where several particles, originally lying flat on the surface adjacent to each other before the RF test, are found arranged one above the other.

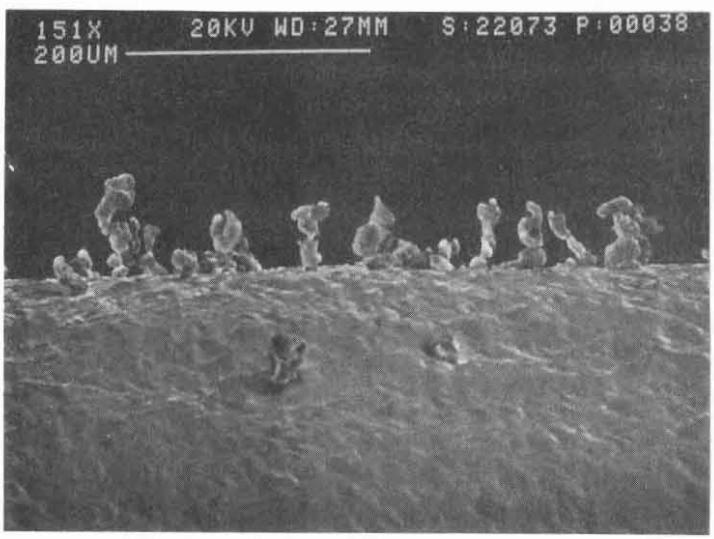

Figure 13: Fe particles found vertically aligned on Thomson cavity finger after RF test.

3. These remaining particles appear all to be lightly welded to the surface, and frequently show signs of melting. Figure 14 shows an example of a welded particle. EDX mapping shows Fe

appearing only on the particle and on the mottled "pedestal" between particle and surface; Nb is detected only on the surface itself.

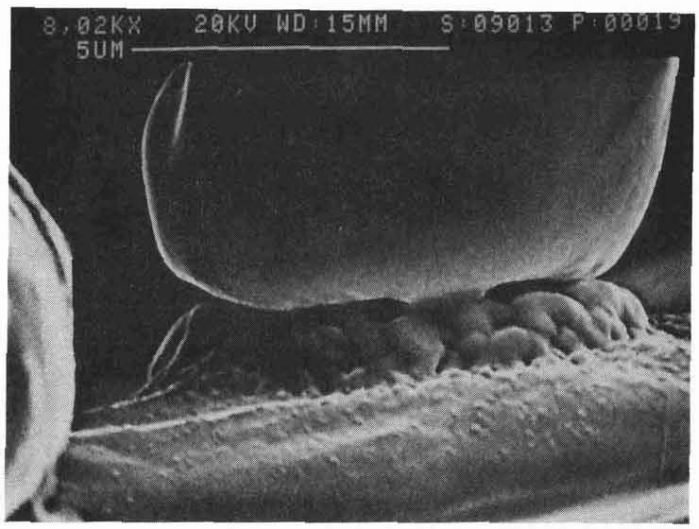

Figure 14: Base of Fe particle found welded to Thomson finger surface after RF test.

DC emission scans of two such Fe-polluted fingers showed that, within the uncertainties of the measurements, the threshold of the most strongly emitting particle was in each case close to the emission threshold previously measured during RF testing[13,14] (see Table 1). Further, these thresholds were both significantly lower than the DC emission thresholds measured for similar Fe particles on flat Nb surfaces and not previously subjected to RF fields.

Table 1: Comparison of FE threshold fields (Fe particles, threshold current 10 nA) for the same Thomson finger in RF and in DC (strongest emitter) after RF.

Sample:	*Nb-1*	*Nb-6*
RF:	14 MV/m	17.5 MV/m
DC:	12 MV/m	19 MV/m

These results show that the forces on a superficial particle due to the RF electric field plays a significant role in the FE process. Like any other conductor, an uncharged metallic particle will polarize in the presence of an electric field. This polarization produces the observed alignment of superficial Fe particles; independent of its sense, an RF cavity field tends to align a polarized elongated particle so that the particle's longest axis is perpendicular to the cavity wall. This realignment in the field may explain the observed tendency for RF FE thresholds to be lower than those for DC; the erect particles in RF produce a larger geometrical field enhancement.

5 CONCLUSIONS

The above results suggest several conclusions regarding the nature and occurrence of RF FE.

5.1 Applicability of projection model

It appears that the classical projection model[1] can explain many instances of RF FE; in particular, that from irregular superficial metal particles. Such particles, upended by the RF field and welded to the cavity surface, are subsequently confirmed to emit in DC. As the main alternatives to the projection model[15] invoke insulating materials or layers, and no such insulators are evident in this emission process, it is difficult to see how these alternative mechanisms could be applicable here.

5.2 Identity of DC and RF field emission

The good agreement between thresholds measured with DC and RF for the same emission sites after exposure to RF suggest that the same basic emission mechanism operates in both domains. Any apparent differences seem explainable by prior RF effects unrelated to emission, such as particle reorientation and melting.

5.3 The danger of metal particle contamination

Demonstrated RF FE from superficial Fe particles, together with DC studies[3] showing that other kinds of metallic particles are also strong emitters, suggest that these particles are particularly to be avoided in the assembly and operation of high-field RF devices. Insulating particles in general appear to be much less dangerous.

5.4 A model for RF processing

The above results suggest a model for the behavior and evolution of a common (though perhaps not the only) type of RF FE site: An irregular metallic particle falls on a high-field region of the cavity wall. Upended and heated by the RF field during a test, it becomes anchored to the wall. The large geometric field enhancement caused by the combination of the upending of the particle and its intrinsically irregular form leads to increasing FE as the RF field increases. Eventually the emission turns into a spark as the metal (and perhaps adsorbed gases) at the emitting tip of the particle vaporizes, forming a localized plasma; in this violent process the entire particle is melted or vaporized, leaving a crater containing traces of the particle's matter melted into the Nb cavity wall. The crater itself may continue to emit, and indeed may emit more vigorously than the original particle; composed mainly of the higher melting point Nb, the crater may also prove harder to destroy (process) than the original particle.

The observation that short RF pulses are more effective than long pulses in processing away superficial metallic contaminants suggests that the details of a particular processing technique may be important in maximizing its effectiveness.

ACKNOWLEDGMENTS

I thank my colleagues at Cornell, Saclay, and Carleton for many useful discussions and for their help in supplying many of the figures used in this paper.

REFERENCES

1. R. J. Noer (1982). *Applied Physics A* **28**, 1.

2. E. Mahner, N. Minatti, H. Piel and N. Pupeter (1993). *Applied Surface Science* **67**, 23.

3. M. Jimenez, R. J. Noer, G. Jouve, C. Antoine, B. Bonin and J. Jodet (1993). *J. Phys. D: Applied Physics,* in press.

4. M. Jimenez, R. J. Noer, G. Jouve, J. Jodet and B. Bonin (1993), submitted for publication.

5. D. L. Moffat et al (1989). *Proceedings of the 4th Workshop on RF Superconductivity*, KEK, Tsukuba, Japan, p. 445. Also distributed as internal report CLNS 89-934.

6. D. Moffat et al (1992). *Particle Accelerators* **40**, 85.

7. J. Tan, H. Safa, B. Bonin, M. Jimenez and J.-M. Tessier (1993), submitted for publication.

8. T. Junquera, A. LeGoff, B. Bonin, H. Safa and J. Tan (1993). *Proceedings of the 6th Workshop on RF Superconductivity*, CEBAF, Newport News, VA, USA.

9. J. Graber (1993). Ph.D. Dissertation, Cornell University.

10. Q. S. Shu et al (1989). *Nuc. Instr. and Methods in Phys.* **A278**, 329.

11. M. Jimenez and R. J. Noer, unpublished work at Saclay

12. T. Hayes, M. Klauda, J. Knobloch, D. Moffat, H. Padamsee, S. Durbin and M. Gray (1993). *Proceedings of the 6th Workshop on RF Superconductivity*, CEBAF, Newport News, VA, USA.

13. J. Tan et al, to be published.

14. GECS-Saclay (1993). *Proceedings of the 6th Workshop on RF Superconductivity*, CEBAF, Newport News, VA, USA.

15. R. V. Latham and N. S. Xu (1991). *Vacuum* **42**, 1173.